processes

MDPI

Article

Insights into Thermal Degradation Behaviors and Reaction Kinetics of Medical Waste Infusion Bag and Nasal Oxygen Cannula

Lifan Zhang [1], Jiajia Jiang [1,2,*], Tengkun Ma [1], Yong Pan [1,2,*], Yanjun Wang [1,2] and Juncheng Jiang [1,2]

[1] College of Safety Science and Engineering, Nanjing Tech University, Nanjing 210009, China; LifanZhang567@126.com (L.Z.); TengkunMa567@126.com (T.M.); yjwang17@outlook.com (Y.W.); jcjiang@njtech.edu.cn (J.J.)
[2] Jiangsu Key Laboratory of Hazardous Chemicals Safety and Control, Nanjing 210009, China
* Correspondence: jiajiajiang@njtech.edu.cn (J.J.); yongpan@njtech.edu.cn (Y.P.)

Abstract: The thermal degradation behaviors and reaction kinetics of medical waste infusion bag (IB) and nasal oxygen cannula (NOC) were investigated under inert atmosphere with the heating rates of 5, 10, 15, and 25 K·min^{-1}. Ozawa–Flynn–Wall (OFW), Kissinger–Akahira–Sunose (KAS), and Friedman were employed to estimate the activation energy. Coats–Redfern and Kennedy–Clark methods were adopted to predict the possible reaction mechanism. The results suggested that the reaction mechanism of IB pyrolysis was zero-order, and that of NOC pyrolysis was concluded that zero-order for the first stage and three-dimensional diffusion Jander equation for the second stage. Based on the kinetic compensation effect, the reconstructed reaction models for IB and NOC pyrolysis were elaborated by introducing adjustment functions. The results indicated that the reconstructed model fitted well with the experimental data. The results are helpful as a reference and provide guidance for the determination of IB and NOC degradation behaviors and the simulation of parameters.

Keywords: medical plastic waste; thermal degradation; thermogravimetric; activation energy; reaction mechanism

Citation: Zhang, L.; Jiang, J.; Ma, T.; Pan, Y.; Wang, Y.; Jiang, J. Insights into Thermal Degradation Behaviors and Reaction Kinetics of Medical Waste Infusion Bag and Nasal Oxygen Cannula. *Processes* **2021**, *9*, 27. https://dx.doi.org/10.3390/pr9010027

Received: 27 October 2020
Accepted: 22 December 2020
Published: 24 December 2020

1. Introduction

Medical waste refers to the hazardous waste generated by hospitals, clinics, or other related medical institutions, which typically contains a variety of potentially infectious and toxic substances [1,2]. There are many types of medical waste, including organic garbage, paper, glass, metal, textile fiber, wood timber, and medical plastic waste, of which medical plastic waste accounts for the highest proportion [3]. Medical waste would not only occupy a large amount of storage space, but also carry a variety of germs. The common way to dispose medical waste is pyrolysis. The three major products that are produced during pyrolysis are oil, gas, and char which are valuable for industries especially production [4]. In addition, pyrolysis is also very flexible since the process parameters can be manipulated to optimize the product yield based on preferences. The liquid oil produced can be used in multiple applications such as furnaces, boilers, turbines, and diesel engines without the needs of upgrading or treatment [5]. Unlike recycling, pyrolysis does not cause water contamination and is considered as green technology when even the pyrolysis by product which is gaseous has substantial calorific value that it can be reused to compensate the overall energy requirement of the pyrolysis plant [6]. So, it is important to investigate the pyrolysis process of medical plastic waste.

The thermal degradation behavior and thermal risk of traditional polymers has attracted lots of attention of many researchers, among which the research on polypropylene and polyvinyl chloride is common. Wang et al. investigated the activation energy of polyvinyl chloride by several commonly-used iso-conversional methods including

Kissinger-Akahira-Sunose (KAS) method, Ozawa-Flynn-Wall (OFW) method, and Friedman method [7]. Aboulkas et al. studied the pyrolysis behavior of polypropylene [8]. The activation energies and pyrolysis kinetic models of polypropylene were obtained. Xu et al. explored the pyrolysis kinetic parameters of polypropylene and polyvinyl chloride by OFW method, KAS method, and Friedman method under high heating rate conditions [9]. Then, the reaction models were calculated by the commonly used model-fitting methods including Coats–Redfern method and Criado method. Han et al. conducted the pyrolysis experiments on polyvinyl chloride in air and nitrogen. The results show that the oxygen in air affected the second stage more obviously than that of the first one, in comparison with nitrogen atmosphere [10]. Nisar et al. revealed pyrolysis kinetics of polypropylene over zeolite modernite using thermogravimetry [11]. The activation energies calculated by three different methods were found in accord with each other. Generally, combining model-free and model-fitting methods together, the kinetic parameters and reaction model of polymers pyrolysis could be obtained thoroughly.

Recently, thermal degradation behavior of medical wastes in polymer have been studied by some researchers. Archibald et al. investigated the flame spread and resistance to ignition of eight fiber reinforced composite mainly composed of polymer [12]. The thermal stability and fire hazard of epoxy polymer pastes was studied by Ushkov et al. [13]. Hassel et al. evaluated the flammability, explosiveness, and vapor pressure of polymer by using differential scanning calorimetry, thermogravimetric analysis, and evolved gas analysis [14]. Deng et al. carried out thermogravimetric analysis under nitrogen atmosphere to obtain pyrolysis kinetic parameters of tube for transfusion, sample collector for urine, and one-off medical glove by the Coats-Redfern method [3]. Huang et al. investigated the pyrolysis and oxidation kinetics of saline bottles to obtain the kinetic parameters based on TGA (thermogravimetric analysis) [15]. However, the pyrolysis of medical plastic waste involves complex reaction due to the evolution of different volatile species. Yan et al. performed kinetic analysis of medical respirator pyrolysis to determine the distributed activation energy model based on first-order kinetic expression by a direct search method [16]. Subsequently, Deng et al. established a novel "two-step four-reaction model" to simulate the whole continuous pyrolysis process for the medical transfusion tube waste containing polyvinyl chloride (PVC) [17]. Qin et al. conducted the pyrolysis experiment of plastic infusion bag in a micro-fluidized bed reactor to calculate the activation energy based on the information of evolution gases mixture [18]. Moreover, the optimum chemical reaction model was confirmed by the Coats-Redfern method. The accurate kinetic parameters are very important for the pyrolysis process simulation. Nevertheless, the common reaction mechanisms sometimes fail to match experimental pyrolysis data well, which cannot describe its real pyrolysis mechanism at different conversions. Jiang et al. discovered that the common reaction models cannot fit well with the experimental profile for extruded polystyrene and rigid polyurethane. They developed new modified models accompanied by accommodation function with best fitting coefficient [19].

In order to obtain the kinetic triplets of thermal degradation more accurately and systematically, two common medical plastic wastes, infusion bag and nasal oxygen tube, were used as the research objects for the pyrolysis experiments under inert atmospheres at different heating rates by thermogravimetric analysis. OFW method, KAS method, and Friedman method were used to calculate the activation energy values of infusion bag and nasal oxygen tube pyrolysis. Coats-Redfern method and Kennedy-Clark method were used to predict the reaction models of infusion bag and nasal oxygen tube preliminarily, then the kinetic compensation effects and the optimal solution to Arrhenius parameters were combined to perform the model reconstruction for confirming the reaction model accurately and systematically. The results of this study would be useful to provide valuable information to reveal the development course of the pyrolysis and combustion of medical plastic waste such as infusion bag and nasal oxygen tube.

2. Materials and Methods

2.1. Sample Preparation

The samples used in this experiment are infusion bag (IB) and nasal oxygen cannula (NOC), which come from Integrated Traditional Chinese and Western Medicine Hospital of Jiangsu Province, China. The main components of IB and NOC are polypropylene and polyvinyl chloride, respectively. For avoiding the influence of moisture and the temperature gradient within the particles of samples, the samples were ground to a particle size of 0.5 mm and then dried in an oven at 373 K for 6 h. The proximate analysis and ultimate analysis of the samples are shown in Table 1. The proximate analysis was performed according to the Chinese National Standards (GB/T 212-2008) and the ultimate analysis was measured by an elemental analyzer (Elementar, Frankfurt, Germany).

Table 1. Proximate analysis and ultimate analysis of samples.

Sample	IB	NOC
Proximate analysis/%		
Ash	0.05	0.10
Volatile matter	98.67	92.26
Fixed carbon [a]	1.28	7.64
Ultimate analysis%		
Carbon	85.59	51.94
Hydrogen	13.78	7.05
Sulfur	0.22	0.37
Oxygen	0.35	0.44
Nitrogen	–	–
Chlorine	–	32.76

[a] By difference.

2.2. Thermogravimetric Experiments

The thermogravimetric experiments were carried out in a thermal analyzer (METTLER TOLEDO, Zurich, Switzerland) with nitrogen (N_2) atmosphere. The temperature increased from 308 to 1173 K at different heating rates of 5, 10, 15, and 25 K·min^{-1}, respectively. The flow rate of ultrahigh purity nitrogen (99.999% N_2) was maintained constantly at 80 mL·min^{-1}. Approximately 10 mg of sample was placed in an alumina crucible for each experiment.

In this study, the reproducibility of the experiments is acceptable and the thermal analysis data corresponding to the different heating rates are the average of runs carried out two times.

2.3. Theoretical Method

Generally, the conversion of polymer pyrolysis can be written as follow:

$$\alpha = \frac{w_0 - w_t}{w_0 - w_f}, \quad (1)$$

where w_0, w_t, and w_f refer to the mass of sample at the initial time, time t, and final time, respectively. The rate of conversion can be expressed by the following basic rate equation:

$$\frac{d\alpha}{dt} = K(T)f(\alpha), \quad (2)$$

where $K(T)$ and $f(\alpha)$ refer to the temperature dependence of the rate of mass loss and the mathematical model that describes the pyrolysis reaction, respectively. $K(T)$ could be obtained by Arrhenius equation:

$$K(T) = Ae^{-\frac{E_a}{RT}}, \quad (3)$$

where E_a is the activation energy, A is the pre-exponential factor, R is the gas constant (8.314 J mol^{-1} K^{-1}), and T is the reaction temperature.

In a non-isothermal linear heating experiment, $\beta = \frac{dT}{dt}$. By combining Equations (2) and (3), the reaction rate can be written in the following form:

$$\beta \frac{d\alpha}{dT} = Ae^{-\frac{E_a}{RT}} f(\alpha). \quad (4)$$

Equation (4) can be transformed to Equation (5):

$$\frac{d\alpha}{f(\alpha)} = \frac{A}{\beta} e^{-\frac{E_a}{RT}} dT. \quad (5)$$

Based on the assumption of $\alpha = \int_0^\alpha \frac{d\alpha}{df(\alpha)}$, Equation (5) can be expressed as the following formula:

$$G(\alpha) = \int_0^\alpha \frac{d\alpha}{f(\alpha)} = \frac{A}{\beta} \int_{T_0}^T exp\left(-\frac{E_a}{RT}\right) dT = \frac{AE_a}{\beta R} p\left(\frac{E_a}{RT}\right). \quad (6)$$

There are two common pyrolysis kinetics research methods in the non-isothermal linear heating experiments, which are the model-free method and model-fitting method [20]. The mode−free methods are used widely to calculate the activation energy of non-isothermal reaction processes for the advantage of requiring no model, but it cannot confirm the kinetic models alone [21,22]. The model-fitting methods are usually used to obtain the kinetic parameters of the reaction through a preselected model [23,24]. Thus, the results show a strong dependence on the mechanism function. In this study, the model-free methods are used combined with the model-fitting methods. The methods including Ozawa−Flynn−Wall (OFW) method [25,26], Kissinger-Akahira-Sunose (KAS) method [27,28] Friedman (FR) method [29], Coats-Redfern (CR) method, and Kennedy-Clark (KC) method [30,31].

2.3.1. Model-Free Method

Equation (6) can be written in the form:

$$\beta = \frac{AE_a}{RG(\alpha)} p\left(\frac{E_a}{RT}\right). \quad (7)$$

The expression of OFW method can be derived by integrating Equation (7) and combining Doyle's approximation ($\ln p\left(\frac{E_a}{RT}\right) \approx -5.331 - 1.052\frac{E_a}{RT}$) [32]:

$$\ln \beta = \ln \frac{AE_a}{RG(\alpha)} - 5.331 - 1.052\frac{E_a}{RT}. \quad (8)$$

Another approximation named Coats–Redfern approximation is used in the Kissinger-Akahira-Sunose (KAS) method:

$$\mathrm{p}\left(\frac{E_a}{RT}\right) = \frac{e^{-\frac{E_a}{RT}}}{(E_a/RT)^2}. \quad (9)$$

The KAS equation can be obtained by combining the Equation (6) and Equation (9):

$$\ln\left(\frac{\beta}{T^2}\right) = \ln\left[\frac{AR}{E_a G(\alpha)}\right] - \frac{E_a}{RT}. \quad (10)$$

Friedman method is a differential iso-conversional method whose expression can be obtained based on Equation (4):

$$\ln\left(\beta\frac{d\alpha}{dT}\right) = \ln[Af(\alpha)] - \frac{E_a}{RT}. \tag{11}$$

2.3.2. Model-Fitting Method

Based on Equation (6) and Equation (9), the expression of the CR method can be obtained by using the asymptotic approximation ($2RT/E_a \ll 1$):

$$\ln\left(\frac{G(\alpha)}{T^2}\right) = \ln\left(\frac{AR}{\beta E_a}\right) - \frac{E_a}{RT}, \tag{12}$$

where $G(\alpha)$ refers to the reaction model.

Table 2 shows 19 classical reaction models applied to describe the pyrolysis process of matters.

Table 2. Commonly-used classical reaction models applied to describe the pyrolysis process of matters.

No	Reaction Model	Symbol	$f(\alpha)$	$G(\alpha)$
1	First-order	F1	$1-\alpha$	$-\ln(1-\alpha)$
2	Three-halves order	F3/2	$(1-\alpha)^{\frac{3}{2}}$	$2\left[(1-\alpha)^{-\frac{1}{2}}-1\right]$
3	Second-order	F2	$(1-\alpha)^2$	$(1-\alpha)^{-1}-1$
4	Third-order	F3	$(1-\alpha)^3$	$\frac{1}{2}\left[(1-\alpha)^{-2}-1\right]$
5	One-dimensional diffusion	D1	$\frac{1}{2}\alpha^{-1}$	α^2
6	Two-dimensional diffusion Valensi equation	D2	$[-\ln(1-\alpha)]^{-1}$	$[(1-\alpha)\ln(1-\alpha)]+\alpha$
7	Three-dimensional diffusion Jander equation	D3	$\frac{3}{2}(1-\alpha)^{\frac{2}{3}}\left[1-(1-\alpha)^{\frac{1}{3}}\right]^{-1}$	$\left[1-(1-\alpha)^{\frac{1}{3}}\right]^2$
8	Three-dimension diffusion G-B equation	D4	$\frac{3}{2}\left[(1-\alpha)^{-\frac{1}{3}}-1\right]^{-1}$	$1-\frac{2}{3}\alpha-(1-\alpha)^{\frac{2}{3}}$
9	Avrami–Erofeev (n = 1.5)	A3/2	$\frac{3}{2}(1-\alpha)[-\ln(1-\alpha)]^{\frac{1}{3}}$	$[-\ln(1-\alpha)]^{\frac{2}{3}}$
10	Avrami–Erofeev (n = 2)	A2	$2(1-\alpha)[-\ln(1-\alpha)]^{\frac{1}{2}}$	$[-\ln(1-\alpha)]^{\frac{1}{2}}$
11	Avrami–Erofeev (n = 3)	A3	$3(1-\alpha)[-\ln(1-\alpha)]^{\frac{2}{3}}$	$[-\ln(1-\alpha)]^{\frac{1}{3}}$
12	Avrami–Erofeev (n = 4)	A4	$4(1-\alpha)[-\ln(1-\alpha)]^{\frac{3}{4}}$	$[-\ln(1-\alpha)]^{\frac{1}{4}}$
13	Zero-order (Polany–Winger equation)	R1	1	α
14	Phase-boundary controlled reaction	R2	$2(1-\alpha)^{\frac{1}{2}}$	$\left[1-(1-\alpha)^{\frac{1}{2}}\right]$
15	Phase-boundary controlled reaction	R3	$3(1-\alpha)^{\frac{2}{3}}$	$\left[1-(1-\alpha)^{\frac{1}{3}}\right]$
16	Power law	P1	$4\alpha^{\frac{3}{4}}$	$\alpha^{\frac{1}{4}}$
17	Power law	P2	$3\alpha^{\frac{2}{3}}$	$\alpha^{\frac{1}{3}}$
18	Power law	P3	$2\alpha^{\frac{1}{2}}$	$\alpha^{\frac{1}{2}}$
19	Power law	P4	$\frac{2}{3}\alpha^{-\frac{1}{2}}$	$\alpha^{\frac{3}{2}}$

Kennedy and Clark developed the KC method based on constant heating rate conditions:

$$T = \beta t + T_0. \tag{13}$$

The basic expression of the KC method can be obtained as follows:

$$\beta G(\alpha)/(T-T_0) = Ae^{\frac{-E_a}{RT}}. \tag{14}$$

By taking the natural logarithm for both sides of Equation (14), the following equation can be obtained:

$$\ln[\beta G(\alpha)/(T-T_0)] = \ln A - \frac{E_a}{RT}. \tag{15}$$

3. Results and Discussion

3.1. Thermogravimetric and Differential Thermogravimetry Analysis

Thermogravimetric (TG) and differential thermogravimetry (DTG) curves of IB and NOC at different heating rates (5, 10, 15, and 25 K·min^{-1}) under a nitrogen environment are shown in Figures 1 and 2. There is only one obvious mass loss stage and one pyrolysis peak for IB, which is different from NOC with two distinct mass loss stages and two pyrolysis peaks. It can be concluded that there are one and two pyrolysis stages for IB and NOC pyrolysis, respectively. Previous studies show there are one and two weightlessness stages for PP and PVC pyrolysis, respectively [8,9,33,34]. The results are consistent with the results obtained of IB and NOC pyrolysis. Although IB and NOC contain some other non-polypropylene and non-polyvinyl chloride substances, the changes in weight are not influenced by them during the pyrolysis process.

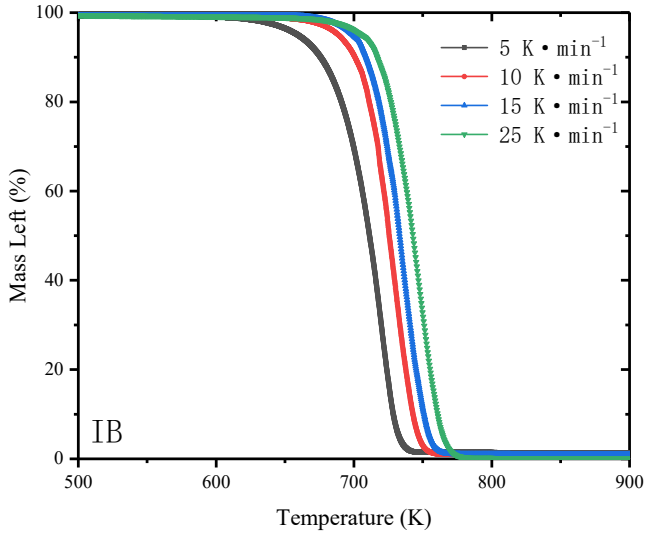

(**a**)

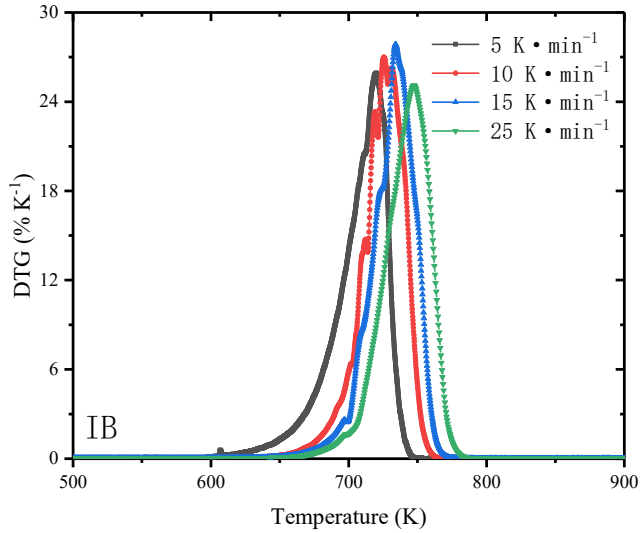

(**b**)

Figure 1. Thermogravimetric and Differential Thermogravimetry curves of infusion bag pyrolysis at different heating rates: (**a**) Thermogravimetric curves; (**b**) Differential Thermogravimetry curves.

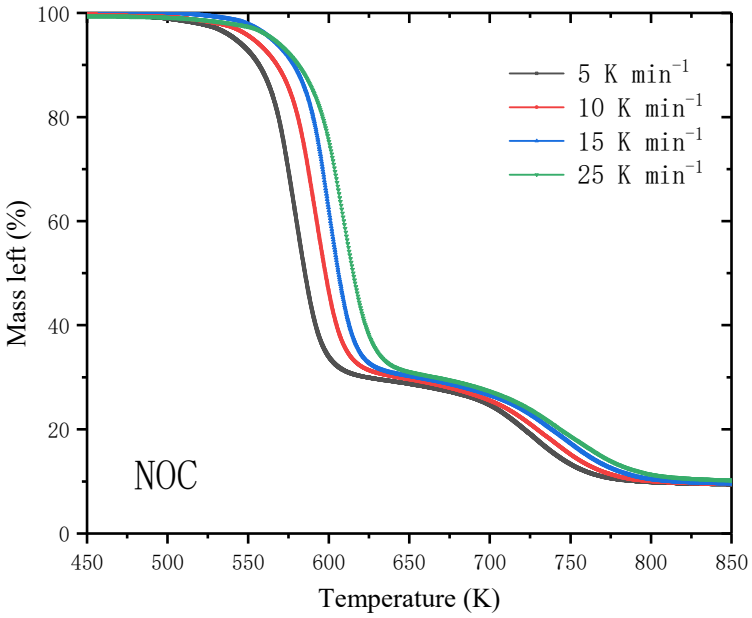

(**a**)

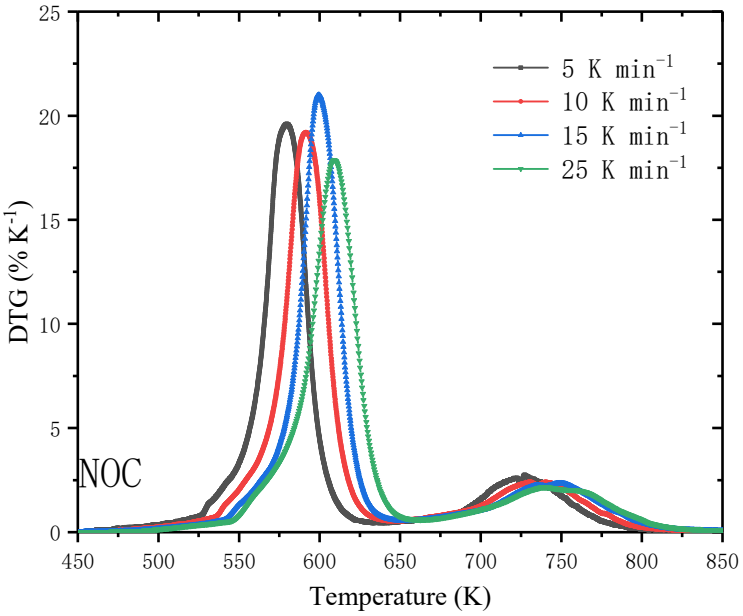

(**b**)

Figure 2. Thermogravimetric and differential thermogravimetry curves of nasal oxygen cannula pyrolysis at different heating rates: (**a**) Thermogravimetric curves; (**b**) Differential Thermogravimetry curves.

Table 3 displays the pyrolysis characteristics of IB and NOC at different heating rates. It can be observed that the pyrolysis temperature range of IB at different heating rates is about 638 to 783 K with mass loss of around 99%. For NOC pyrolysis, the first stage took place in the range of 494 to 650 K with the mass loss of about 69%. The second stage occurred at 619 K and finished at 810 K with the mass loss of 91% approximately. Two different pyrolysis peaks can be observed obviously in the DTG curves of NOC, which may be caused by the reason that C-Cl with lower dissociation energy would break earlier

than C-C, C-H, and C=C when polyvinyl chloride is pyrolyzed. The dissociation energies of C-Cl, C-C, C-H, and C=C are 339, 347, 414, and 611 kJ·mol^{-1}, respectively [9].

Combined with the data in Table 3, it can be concluded that the initial, end, and maximum weight loss temperature of IB and NOC pyrolysis show a lateral shift to a higher temperature. Many researchers considered that the phenomenon occurred because of the heat transfer limitations and thermal lag [35]. The thermal lag means that there had a large difference between furnace temperature and sample temperature, which is more obvious at high heating rates [36].

Table 3. Pyrolysis characteristics of infusion bag and nasal oxygen cannula at different heating rates.

Sample	Heating Rate/K min^{-1}		Pyrolysis Interval/K	Peak Temperature/K	Mass Loss/%
IB	5		638–745	722	98.48
	10		649–761	727	99.18
	15		656–772	734	99.24
	25		665–783	747	99.96
NOC	5	First Stage	494–619	580	69.37
		Second Stage	619–772	726	91.11
	10	First Stage	507–630	592	69.14
		Second Stage	630–786	738	91.18
	15	First Stage	532–638	599	69.04
		Second Stage	638–802	749	91.11
	25	First Stage	548–650	609	68.94
		Second Stage	650–810	758	91.09

3.2. Model-Free Analysis

The energy required for a molecule to change from a normal state to an active state is called activation energy, which is very important for the study of pyrolysis dynamics. In this paper, three different model-free methods including OFW, KAS, and Friedman methods were used to calculate the activation energy.

The activation energy values calculated by the three different methods show the similar tendency. The activation energy of IB pyrolysis is shown in Figure 3a and the conversion rate is changed from 0.02 to 0.98. The results indicate that the activation energy values vary between 83.93 to 219.30 kJ·mol^{-1} for OFW method, 83.69 to 218.42 kJ·mol^{-1} for KAS method, and 119.15 to 258.01 kJ·mol^{-1} for Friedman method. The average of the values calculated by the three different methods is 202.53 kJ·mol^{-1}.The variation of activation energy for NOC pyrolysis is presented in Figure 3b. With the conversion rate varies from 0.02 to 0.76, the activation energy of the first stage changes from 85.49 to 152.79 kJ·mol^{-1} for OFW method, 81.12 to 151.21 kJ·mol^{-1} for KAS method and 105.99 to 158.50 kJ·mol^{-1} for Friedman method. With the conversion rate varies from 0.78 to 0.98, the activation energy of the second stage varies from 114.87 to 290.20 kJ·mol^{-1} for OFW method, 110.24 to 293.43 kJ·mol^{-1} for KAS method, and 98.28 to 321.71 kJ·mol^{-1} for Friedman method. The average of the values calculated by the three different methods are 146.36 and 257.49 kJ·mol^{-1} for the first and second stages, respectively.

For IB, the values of activation energy increase at the initial stage and then the values show a slightly variation. Previous studies have also calculated the values of activation energy of PP and the results are different. The studies of Xu et al. show that the values of activation energy present a decreasing trend at the end of the pyrolysis process of PP and the values are lower than that of IB [9]. Aboulkas et al. calculated the values of activation energy of PP and the results indicated the values fluctuated around 210 kJ·mol^{-1} during the whole pyrolysis process [8]. For NOC, it can be observed that the activation energy remains constant substantially in the first stage and shows significant variation in the second stage, and the activation energy of the second stage is generally higher than that of the first stage. This can be explained by the reason that when polyvinyl chloride is

pyrolyzed, the chemical bonds broken in the first pyrolysis stage are mainly C-Cl, whereas in the second pyrolysis stage, the broken chemical bonds are mainly C-C, C-H, and C=C whose dissociation energies are all higher than that of C-Cl [9].

It can be observed in Figure 3 that the activation energy values calculated by OFW method and KAS method keep very high consistency, whereas the values obtained by Friedman method are significantly different with other two methods. The difference of the activation energy may be caused by the large data noise during data processing when Friedman method was employed [37].

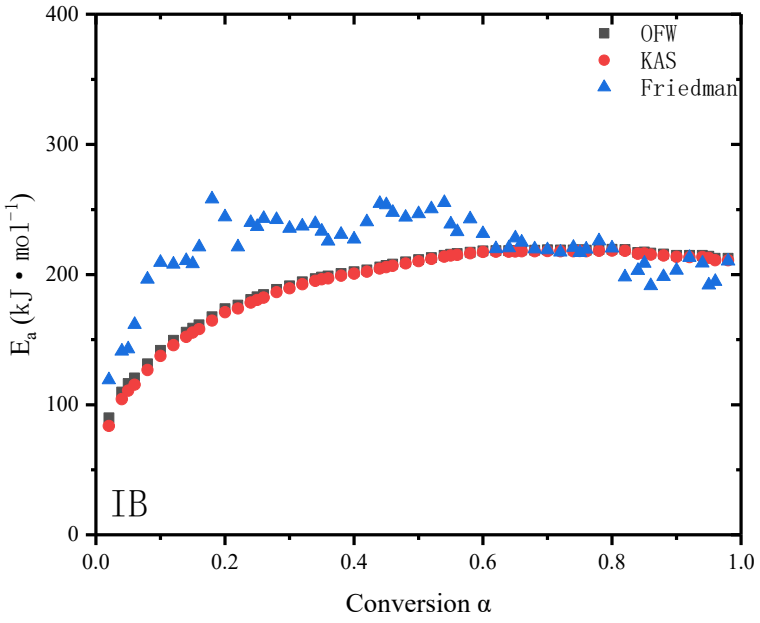

(**a**)

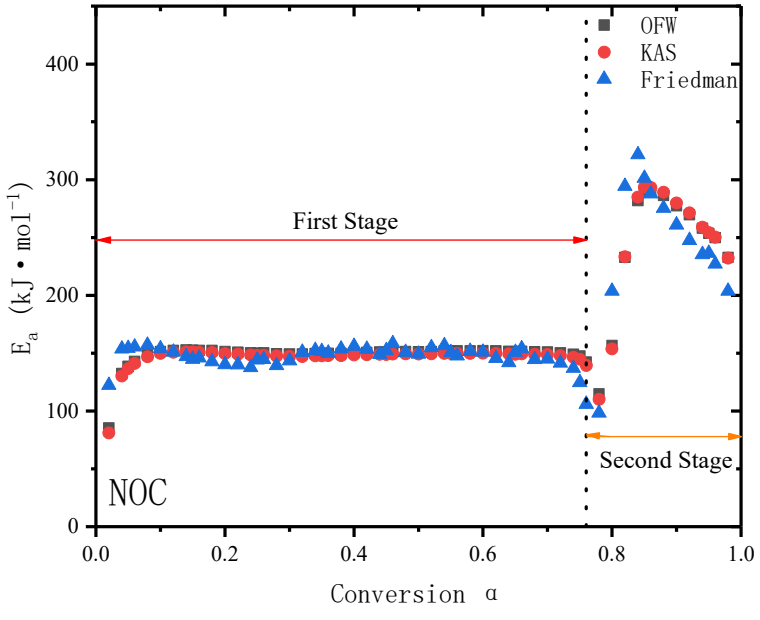

(**b**)

Figure 3. Activation energy values obtained from model-free methods: (**a**) IB, (**b**) NOC.

3.3. Model-Fitting Analysis

The details about the pyrolysis reaction model cannot be obtained by utilizing the model-free method alone. In this paper, the reaction models of IB and NOC during the main pyrolysis interval at different heating rates were explored by model-fitting methods including CR method and KC method with the target models in Table 2. The details of IB and NOC pyrolysis kinetics calculated by CR method and KC method are displayed in Appendix A.

The results indicate that the kinetic parameters including the activation energy and pre-exponential factor corresponding to 19 distinct reaction models are diverse, which means that Arrhenius parameters are strongly dependent on the selected model. The correlation coefficients are greater than 0.9 generally, which indicates that the results obtained by CR method and KC method are dependable. The activation energy and linear coefficient obtained by the model-fitting method are usually used to determine the most probable mechanism function [22,23]. The best selected models for IB and NOC pyrolysis based on model-free method and model-fitting method are present in Table 4.

For IB pyrolysis, the average of the activation energy calculated by model-free methods is 202.53 kJ·mol^{-1}. As presented in Tables A1 and A2, the values of activation energy calculated by model-fitting-methods are quite different. Among the 19 different kinetic models, the value corresponding to R1 (Zero-order) is the closest to the results of the model-free methods. Meanwhile, the correlation coefficients at different heating rates are also close to 1, which means the results are dependable. It can be concluded that R1 is the reaction model for IB pyrolysis. For the first and second pyrolysis stages of NOC, the average of the activation energy calculated by model-free methods are 146.36 kJ·mol^{-1} and 257.49 kJ·mol^{-1}, respectively. As shown in Tables A3–A6, the values of activation energy corresponding to R1 (Zero-order) are the closest to the results of the model-free methods for the first stage and the results of D3 (three-dimensional diffusion Jander equation) are closest for the second stage. At the same time, the correlation coefficients corresponding to the two models at different heating rates are both close to 1, which means the results are reliable. Therefore, R1 and D3 are the reaction model for the first and second pyrolysis stages of NOC, respectively. Xu et al. and Aboulkas et al. thought the kinetic model is R3 (contracting cylinder) for PP pyrolysis [9]. For PVC pyrolysis, Xu et al. thought A2 (two-dimension nucleation) and D3 (three-dimension diffusion: Jander) are the kinetic models for the first and second stages, respectively [9]. The differences in kinetic models may be caused by the reason that IB and NOC contain some other non-polypropylene and non- polyvinyl chloride materials. The kinetic models of PVC studied by Wang et al. are also different, which may be caused by the same reason [7].

However, due to the interference of initial gas flow, the small mass loss at the initial pyrolysis reaction cannot really reflect the pyrolysis mechanism. The reaction models were obtained based on the experimental data of main pyrolysis interval. It should be noted that the selected reaction mechanism models may not describe the whole pyrolysis process well. In order to confirm the reaction course more accurately, the adjustment functions will be introduced to reconstruct the reaction model in the following sections.

Table 4. The kinetic parameters of IB and NOC calculated by Coats-Redfern and Kennedy-Clark methods for the best models which describe the pyrolysis process well at different heating rates.

Sample		Method	Model	5 K·min^{-1}			10 K·min^{-1}			15 K·min^{-1}			25 K·min^{-1}			Average E_a
				E_a	ln A	R^2	E_a	ln A	R^2	E_a	ln A	R^2	E_a	ln A	R^2	
IB		CR method	R1	153.39	23.51	0.99308	213.44	33.84	0.97666	227.19	36.17	0.96492	212.97	33.81	0.97110	201.75
		KC method	R1	154.50	21.01	0.99311	184.39	27.29	0.97102	228.75	33.36	0.96556	214.62	31.08	0.97167	195.57
NOC	First stage	CR method	R1	133.23	25.56	0.98340	132.67	25.51	0.98539	149.08	28.90	0.98270	124.00	23.86	0.98141	134.75
		KC method	R1	132.43	22.83	0.98334	132.10	22.83	0.98539	148.68	26.15	0.98273	123.70	21.31	0.98844	134.23
	Second Stage	CR method	D3	219.24	32.21	0.98953	221.64	32.86	0.99881	223.63	33.17	0.99930	229.49	34.34	0.99697	223.50
		KC method	D3	220.51	29.38	0.98948	223.06	30.04	0.99880	225.16	30.36	0.99929	231.13	31.53	0.99710	224.97

3.4. Kinetic Compensation Effect

There is an interdependence of the characteristic kinetic parameters which is obtained through the non-isothermal experiments. The certain dependence between activation energy and pre-exponential factor is called kinetic compensation effect (KCE) [38], which is useful for the model reconstruction. The expression is listed as follow:

$$\ln A_i = a + bE_{a,i}, \tag{16}$$

where the parameters a and b are reaction compensation parameters, $a = \ln k_{iso}$ and $b = 1/RT_{iso}.k_{iso}$ is artificial isokinetic rate constant, and T_{iso} is artificial isokinetic temperature. The subscript i means the selected model listed in Table 2. If the reaction model is not selected correctly, the artificial isokinetic temperature will deviate out of the actual reaction temperature range [39].

The KCE relationships obtained by CR method and KC method combined with the reaction model in Table 2 are displayed in Figures 4 and 5. The results indicate that the linear relationship between E_a and $\ln A$ are obvious. The KCE can be expressed as $\ln A = -1.767 + 0.1661E_a$ with $R^2 = 0.99829$ for IB pyrolysis, $\ln A = -1.809 + 0.2051E_a$ with $R^2 = 0.99776$, and $\ln A = -2.850 + 0.1694E_a$ with $R^2 = 0.99220$ for the first and second pyrolysis stages of NOC, respectively. With the known KCE expressions, the value of artificial isokinetic rate constant and artificial isokinetic temperature can be calculated. As shown in Table 5, the values of a and b calculated by CR and KC methods are all different at different heating rates. Additionally, all the values of T_{iso} are located within the actual reaction temperature range, which also indicates that the selection of reaction model is proper. In addition, the dependence of $\ln A$ on each conversional extent can also be determined with the expressions of KCE. The $\ln A$ at each conversional extent is shown in Figure 6, where the activation energy is obtained by the model-free methods.

3.5. Model Reconstruction

After combining Equations (2) and (4), the reaction mechanism function can be expressed as follows:

$$f(\alpha) = \frac{\beta}{A}\frac{d\alpha}{dT}e^{\frac{E_a}{RT}}. \tag{17}$$

Based on Sections 3.2–3.4, all the parameters on the right of Equation (17) can be obtained. Then, the value of $f(\alpha)$ can be calculated for each conversion. Therefore, the scatter plot of $f(\alpha)$ on α can be drawn. The accuracy of the obtained reaction model can be verified by this method.

As the aforementioned conclusion in Section 3.3, the reaction models for IB and NOC have been confirmed preliminarily. However, it does not mean that the selected models are the actual reaction models of IB and NOC. The selected model does not necessarily fit well with the experimental data, because the most commonly-used classical reaction models may be not completely suitable for describing the reaction process of solid [40]. Therefore, it is necessary to introduce an adjustment function to modify the known classical reaction models present in Table 2 for reconstructing the reaction model accurately. The adjustment function can be represented by $c\alpha^m$ and the modified function can be expressed by the arithmetic products of the adjustment function and a known reaction model [41]. The new modified models for IB pyrolysis can be expressed by Equation (18):

$$f(\alpha) = c\alpha^m(1-\alpha)^n. \tag{18}$$

The new modified models for the first and second pyrolysis stages of NOC can be expressed by Equations (19) and (20), respectively:

$$f(\alpha) = c\alpha^m(1-\alpha)^n, \tag{19}$$

$$f(\alpha) = c\alpha^m \frac{3}{n}(1-\alpha)^{\frac{2}{3}}\left[1-(1-\alpha)^{\frac{1}{3}}\right]^{1-n}. \quad (20)$$

The values of the three parameters c, m, and n can be obtained based on the known correspondence between $f(\alpha)$ and α in Equation (17). Therefore, the specific mathematical expression of the new modified model can be determined. The comparison results of experimental data with modified model and the selected classical model are shown in Figure 7 and Table 6, where the smaller residual sum of squares (RSS) indicates that the model fit better with the experimental data.

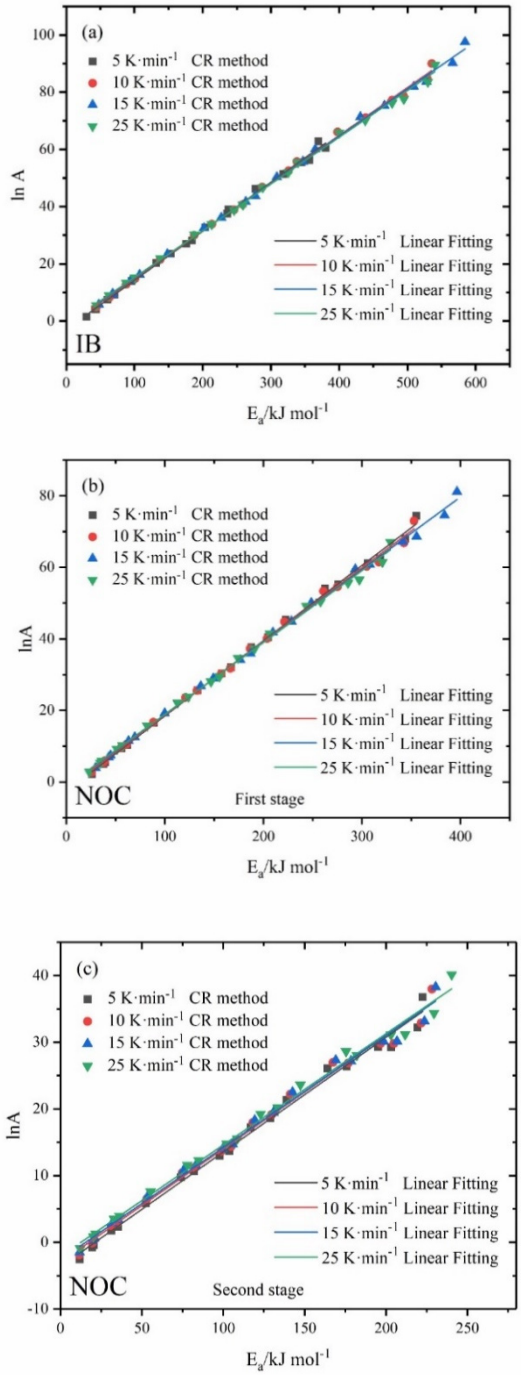

Figure 4. The Kinetic Compensation Effect relationships by CR method at different heating rates: (**a**) IB, (**b**) the first pyrolysis stage of NOC, (**c**) the second pyrolysis stage of NOC.

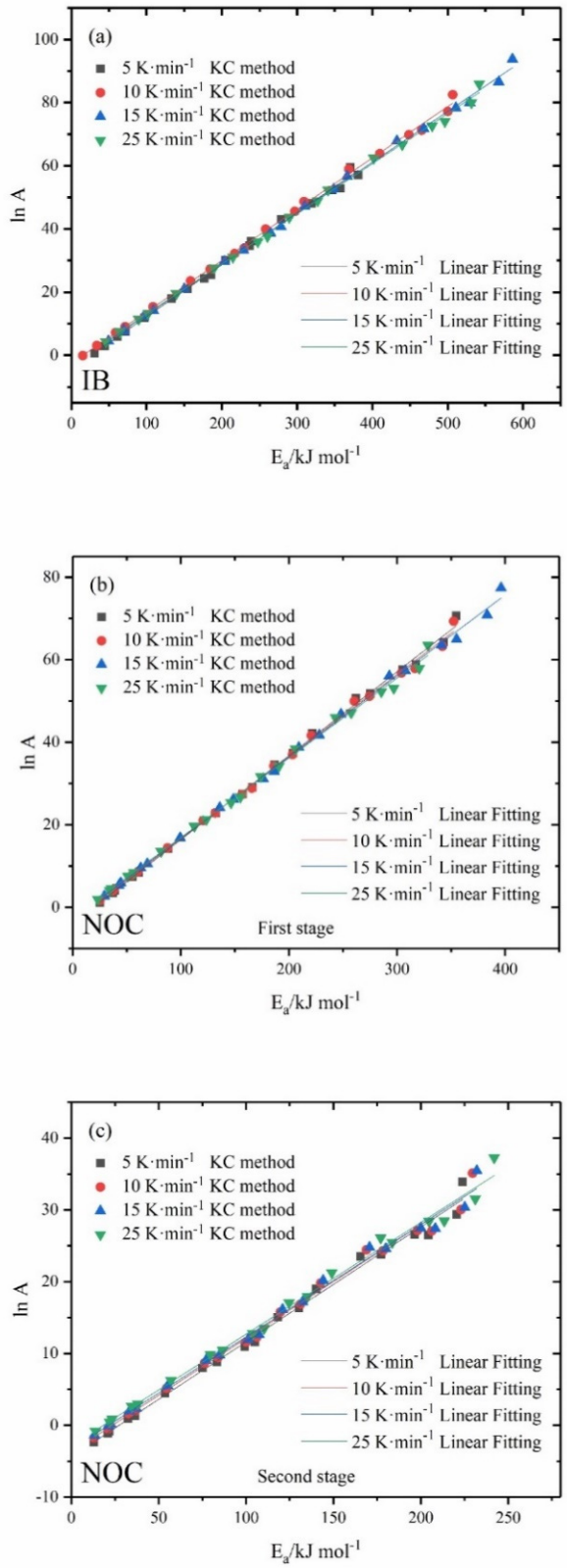

Figure 5. The Kinetic Compensation Effect relationship by Kennedy-Clark method at different heating rates: (**a**) IB, (**b**) the first pyrolysis stage of NOC, (**c**) the second pyrolysis stage of NOC.

Table 5. Artificial isokinetic parameters obtained by using the KCE for IB and NOC pyrolysis at different heating rates.

Sample		β/K·min^{-1}	CR Method					KC Method				
			a/min^{-1}	b/mol kJ^{-1}	k_{iso}/min^{-1}	T_{iso}/K	R^2	a/min^{-1}	b/mol kJ^{-1}	k_{iso}/min^{-1}	T_{iso}/K	R^2
IB		5	−2.874	0.1713	0.05647	702.15	0.99728	−4.282	0.16483	0.01382	729.72	0.99734
		10	−1.899	0.1670	0.14972	720.23	0.99852	−2.496	0.16248	0.08241	740.27	0.99854
		15	−1.468	0.1653	0.23038	727.64	0.99868	−3.309	0.16106	0.03655	746.80	0.99869
		25	−1.042	0.1632	0.35275	737.00	0.99845	−2.805	0.15869	0.06051	757.95	0.99847
NOC	First Stage	5	−2.622	0.2105	0.07266	571.40	0.99802	−3.957	0.20339	0.01912	591.37	0.99804
		10	−1.976	0.2062	0.13862	583.31	0.99792	−3.305	0.19902	0.03670	604.36	0.99794
		15	−1.474	0.2029	0.22901	592.80	0.99828	−2.929	0.19655	0.05345	611.95	0.99830
		25	−1.189	0.2009	0.30453	598.70	0.99750	−2.441	0.1932	0.08707	622.56	0.99752
	Second Stage	5	−3.657	0.1720	0.02581	699.30	0.99279	−4.381	0.16003	0.01251	751.60	0.99265
		10	−2.995	0.1701	0.05004	707.11	0.99282	−3.725	0.15832	0.02411	759.72	0.99262
		15	−2.605	0.1683	0.07390	714.67	0.99279	−3.340	0.15655	0.03544	768.31	0.99258
		25	−2.098	0.1669	0.12270	720.67	0.99308	−2.861	0.15557	0.05721	773.15	0.99282

Sometimes, although the classical reaction models in Table 2 can reveal the reaction mechanism of pyrolysis process, they cannot describe the pyrolysis behaviors accurately. In this paper, after analyzing the reaction process, the models determined by the CR method and KC method were explored furtherly by model reconstruction with adjustment function. The results show that the reconstructed model keeps higher consistency with the experimental data than the models confirmed by model-fitting method. The final pyrolysis models for IB and NOC can provide guidance to medical plastic waste pyrolysis modeling studies.

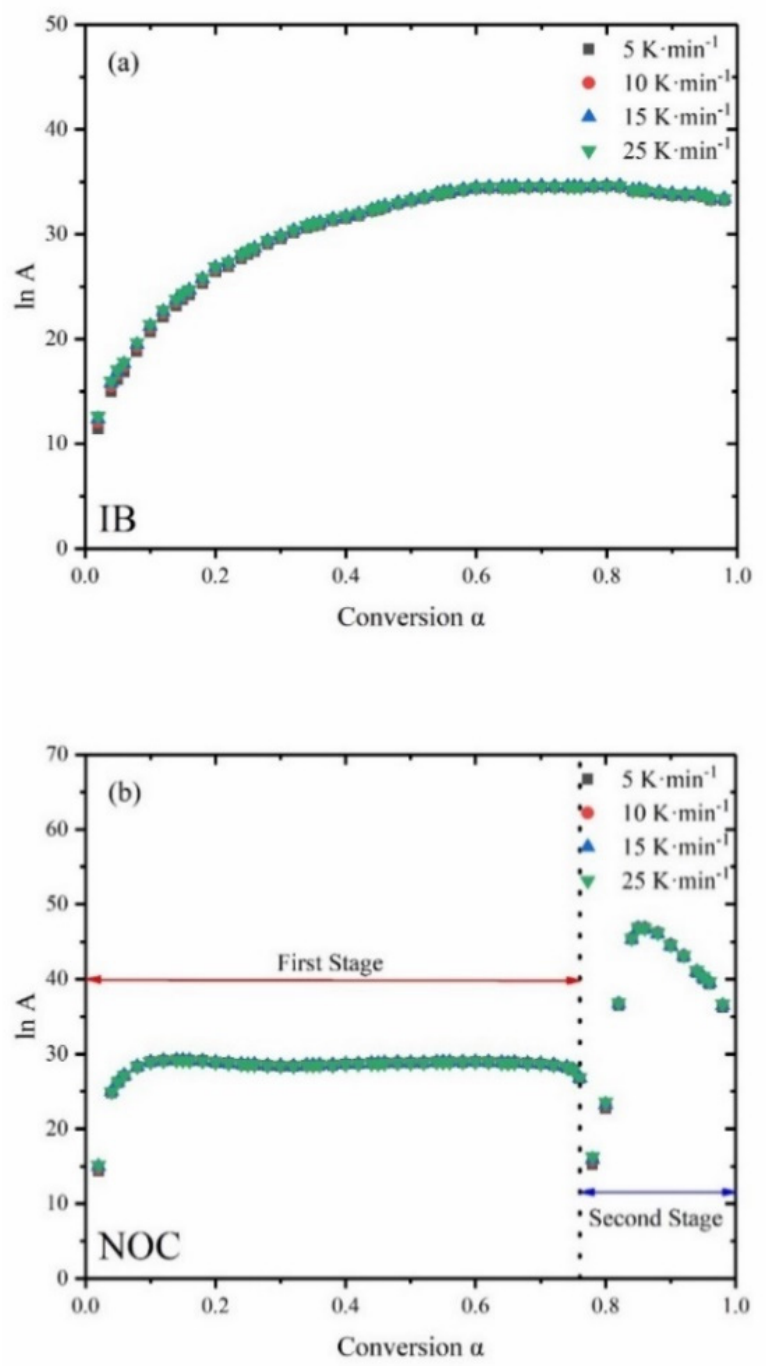

Figure 6. Dependence of pre-exponential factors on conversional extent at different heating rates: (**a**) IB, (**b**) NOC.

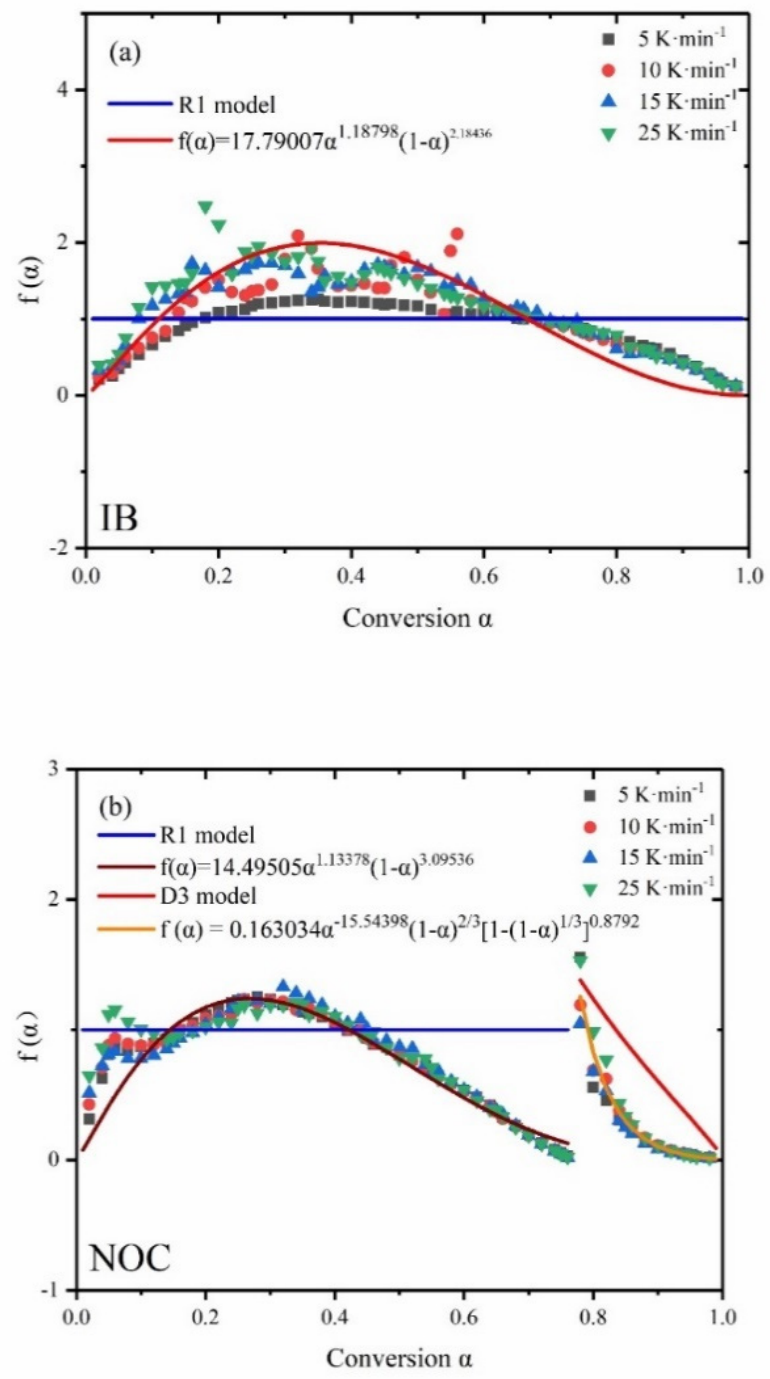

Figure 7. Model reconstruction of the kinetic mechanism function at different heating rates: (**a**) IB, (**b**) NOC.

Table 6. Reconstruction model results of IB and NOC dependent on reaction model.

Sample		Reaction Model	RSS	Modified Model	RSS
IB		R1 (Zero-order)	58.63671	$17.79007\alpha^{1.18798}(1-\alpha)^{2.18436}$	2.10598
NOC	First Stage	R1 (Zero- order)	31.29233	$14.49505\alpha^{1.13378}(1-\alpha)^{3.09536}$	0.25205
	Second Stage	D3 (Three-dimensional diffusion Jander equation)	10.87707	$0.163034\alpha^{-15.54398}(1-\alpha)^{\frac{2}{3}}\left[1-(1-\alpha)^{\frac{1}{3}}\right]^{0.8792}$	0.00207

4. Conclusions

IB and NOC were chosen to investigate the thermal degradation behaviors and kinetic analysis in detail by thermogravimetric. There are one and two stages can be observed for IB and NOC pyrolysis, respectively. The results of model-free methods show that the activation energy values vary between 83.93 to 258.01 kJ·mol^{-1} for IB pyrolysis, 81.12 to 158.50 kJ·mol^{-1} and 98.28 to 321.71 kJ·mol^{-1} for the first and second pyrolysis stages of NOC, respectively. The consequences of model-fitting methods suggest that IB pyrolysis is controlled by zero-order, and NOC pyrolysis is governed by zero-order for the first stage and three-dimensional diffusion Jander equation for the second stage.

The kinetic compensation effect indicates that there is an obvious linear relationship between the pre-exponential factor and activation energy for IB and NOC pyrolysis. The reaction models of IB and NOC pyrolysis are reconstructed by introducing adjustment functions.

The reconstructed reaction models are $f(\alpha) = 17.79007\alpha^{1.18798}(1-\alpha)^{2.18436}$ for IB pyrolysis, $f(\alpha) = 14.49505\alpha^{1.13378}(1-\alpha)^{3.09536}$ and $f(\alpha) = 0.163034\alpha^{-15.54398}(1-\alpha)^{\frac{2}{3}}\left[1-(1-\alpha)^{\frac{1}{3}}\right]^{0.8792}$ for the first and second pyrolysis stages of NOC, respectively. It is anticipated that our current study will provide a route to analyze the pyrolysis kinetic of IB and NOC, and the obtained kinetic triplets could be helpful to further investigate medical plastic wastes pyrolysis in actual disposal scenarios.

Author Contributions: Conceptualization, L.Z., J.J. (Jiajia Jiang) and Y.P.; methodology, L.Z., J.J. (Jiajia Jiang) and T.M.; software, L.Z.; validation, J.J. (Jiajia Jiang) and J.J. (Juncheng Jiang); formal analysis, L.Z.; investigation, L.Z. and J.J. (Jiajia Jiang); resources, L.Z., J.J. (Jiajia Jiang) and Y.P.; data curation, L.Z. and Y.W.; writing—original draft preparation, L.Z.; writing—review and editing, J.J. (Jiajia Jiang), Y.P. and J.J. (Juncheng Jiang); visualization, L.Z.; supervision, T.M. and Y.W.; project administration, J.J. (Jiajia Jiang) and Y.P.; funding acquisition, J.J. (Jiajia Jiang). All authors have read and agreed to the published version of the manuscript.

Funding: This work was supported by National Natural Science Foundation of China (No.51804167, 51974165) and Natural Science Foundation of Jiangsu (No. BK20150953).

Institutional Review Board Statement: Not involving humans or animals.

Informed Consent Statement: Not applicable for studies not involving humans.

Data Availability Statement: No new data were created or analyzed in this study. Data sharing is not applicable to this article.

Conflicts of Interest: The authors declare no conflict of interest.

Appendix A

Table A1. The kinetic parameters of IB calculated by CR method at different heating rates.

Model	5 K·min^{-1}			10 K·min^{-1}			15 K·min^{-1}			25 K·min^{-1}			Average
	E_a/kJ·mol^{-1}	ln A/min^{-1}	R^2	E_a/kJ·mol^{-1}	ln A/min^{-1}	R^2	E_a/kJ·mol^{-1}	ln A/min^{-1}	R^2	E_a/kJ·mol^{-1}	ln A/min^{-1}	R^2	E_a/kJ·mol^{-1}
F1	203.64	32.78	0.96627	287.25	46.83	0.98824	308.66	50.31	0.99768	287.84	46.70	0.99105	271.85
F3/2	237.77	39.01	0.92395	338.06	55.71	0.96566	364.98	60.00	0.98527	339.45	55.51	0.97225	320.07
F2	277.55	46.24	0.87021	397.60	66.07	0.92784	431.07	71.34	0.95559	399.95	65.80	0.93738	376.54
F3	369.55	62.87	0.77075	535.64	89.99	0.84701	584.43	97.55	0.88459	540.25	89.57	0.86009	507.47
D1	318.27	51.40	0.99353	438.77	71.09	0.97795	466.43	75.31	0.96676	438.10	70.17	0.97273	415.39
D2	345.08	55.59	0.99252	477.67	77.20	0.98675	509.22	81.99	0.98142	477.53	76.21	0.98390	452.38
D3	380.15	60.45	0.98436	529.27	84.67	0.99210	566.20	90.26	0.99419	529.88	83.60	0.99214	501.38
D4	356.53	56.17	0.99074	494.50	78.62	0.98957	527.79	83.67	0.98678	494.60	77.61	0.98772	468.36
A3/2	131.94	20.30	0.96458	187.54	30.00	0.98781	201.75	32.46	0.98760	187.84	30.20	0.98072	177.27
A2	96.08	13.96	0.96275	137.68	21.49	0.98736	148.30	23.45	0.99751	137.84	21.85	0.99036	129.98
A3	60.23	7.47	0.9586	87.83	12.83	0.98637	94.85	14.29	0.99733	87.83	13.37	0.98959	82.69
A4	42.30	4.10	0.95365	62.90	8.40	0.98525	68.13	9.61	0.99713	62.83	9.01	0.98871	59.04
R1	153.39	23.51	0.99308	213.44	33.84	0.97666	227.19	36.17	0.96492	212.97	33.81	0.97110	201.75
R2	175.69	26.95	0.99878	245.98	38.90	0.99033	263.04	41.72	0.98885	245.96	38.82	0.98893	232.67
R3	184.34	28.13	0.98356	258.70	40.73	0.99176	277.08	43.75	0.99391	258.86	40.63	0.99178	244.75
P1	29.73	1.50	0.98890	44.45	4.88	0.96614	47.76	5.80	0.95012	44.12	5.51	0.95767	41.52
P2	43.47	4.15	0.99066	63.23	8.27	0.97030	67.70	9.35	0.95591	62.88	8.84	0.96300	59.32
P3	70.95	9.16	0.99202	100.78	14.83	0.97376	107.57	16.22	0.96078	100.40	15.24	0.96741	94.93
P4	235.83	37.52	0.99339	326.11	52.53	0.97753	346.81	55.81	0.96616	325.53	52.06	0.97220	308.57

Table A2. The kinetic parameters of IB calculated by KC method at different heating rates.

Model	5 K·min^{-1}			10 K·min^{-1}			15 K·min^{-1}			25 K·min^{-1}			Average
	E_a/kJ·mol^{-1}	ln A/min^{-1}	R^2	E_a/kJ·mol^{-1}	ln A/min^{-1}	R^2	E_a/kJ·mol^{-1}	ln A/min^{-1}	R^2	E_a/kJ·mol^{-1}	ln A/min^{-1}	R^2	E_a/kJ·mol^{-1}
F1	204.75	29.99	0.96627	258.19	39.98	0.98177	310.22	47.18	0.99768	289.49	43.66	0.99106	265.66
F3/2	238.88	36.07	0.92420	309.01	48.70	0.95425	366.54	56.71	0.98531	341.10	52.31	0.97236	313.88
F2	278.66	43.15	0.87072	368.55	58.89	0.91187	432.63	67.88	0.95578	401.60	62.43	0.93769	370.36
F3	370.66	59.49	0.77150	506.59	82.52	0.82769	586.00	93.79	0.88501	541.91	85.90	0.86067	501.29
D1	319.37	48.17	0.99354	409.71	63.82	0.97571	467.99	71.78	0.96706	439.76	66.71	0.97299	409.21
D2	346.18	52.28	0.99248	448.62	69.84	0.98505	510.78	78.37	0.98158	479.18	72.66	0.98404	446.19
D3	381.26	57.05	0.98432	500.21	77.20	0.99028	567.76	86.53	0.99424	531.53	79.96	0.99217	495.19
D4	357.64	52.83	0.99069	465.44	71.23	0.98794	529.35	80.01	0.98690	496.25	74.03	0.98781	462.17
A3/2	133.04	17.95	0.96459	158.49	23.57	0.97632	203.32	29.77	0.98760	189.49	27.59	0.98074	171.09
A2	97.19	11.93	0.96278	108.63	15.37	0.96898	149.87	21.06	0.99752	139.49	19.55	0.99041	123.80
A3	61.33	5.90	0.95873	58.78	7.17	0.94488	96.42	12.35	0.99734	89.49	11.52	0.98968	76.51
A4	43.41	2.89	0.95398	33.85	3.06	0.89514	69.69	8.00	0.99715	64.49	7.50	0.98886	52.86
R1	154.50	21.01	0.99311	184.39	27.29	0.97102	228.75	33.36	0.96556	214.62	31.08	0.97167	195.57
R2	176.80	24.31	0.99868	216.93	32.20	0.99631	264.60	38.76	0.99005	247.61	35.94	0.99052	226.49
R3	185.44	25.45	0.98347	229.64	33.98	0.98736	278.64	40.73	0.99401	260.51	37.70	0.99186	238.56
P1	30.84	0.64	0.98928	15.40	−0.11	0.79284	49.33	4.54	0.95403	45.77	4.35	0.96129	35.34
P2	44.58	2.91	0.99085	34.18	2.94	0.91564	69.26	7.74	0.95843	64.53	7.32	0.96529	53.14
P3	72.06	7.43	0.99210	71.73	9.02	0.95469	109.13	14.15	0.96224	102.05	13.26	0.96872	88.74
P4	236.94	34.59	0.99340	297.05	45.55	0.97431	348.37	52.57	0.96657	327.19	48.89	0.97256	302.39

Table A3. The kinetic parameters of the first pyrolysis stage of NOC calculated by CR method at different heating rates.

Model	5 K·min^{-1}			10 K·min^{-1}			15 K·min^{-1}			25 K·min^{-1}			Average
	E_a/kJ·mol^{-1}	ln A/min^{-1}	R^2	E_a/kJ·mol^{-1}	ln A/min^{-1}	R^2	E_a/kJ·mol^{-1}	ln A/min^{-1}	R^2	E_a/kJ·mol^{-1}	ln A/min^{-1}	R^2	E_a/kJ·mol^{-1}
F1	187.61	37.64	0.99052	186.65	37.28	0.98944	209.65	41.83	0.98989	174.28	34.60	0.98600	189.55
F3/2	222.60	45.35	0.97856	221.37	44.78	0.97607	248.64	50.08	0.97818	206.57	41.42	0.96969	224.80
F2	262.64	54.12	0.95969	261.07	53.31	0.95603	293.26	59.48	0.95959	243.49	49.19	0.94719	265.12
F3	355.30	74.34	0.91678	352.95	72.96	0.91148	396.53	81.15	0.91710	328.86	67.04	0.89930	358.41
D1	275.97	55.25	0.98456	275.05	54.51	0.98644	308.03	60.80	0.98383	257.96	50.42	0.98932	279.25
D2	306.05	61.17	0.99056	304.93	60.26	0.99156	341.52	67.18	0.98977	285.82	55.60	0.99259	309.58
D3	343.95	67.96	0.99334	342.55	66.83	0.99328	383.74	74.57	0.99261	320.86	61.45	0.99207	347.78
D4	318.52	62.40	0.99218	317.31	61.42	0.99281	355.42	68.61	0.99141	297.36	56.52	0.99306	322.15
A3/2	121.90	23.64	0.99008	121.20	23.61	0.98893	136.48	26.81	0.98944	112.87	22.09	0.98526	123.11
A2	89.05	16.54	0.98960	88.47	16.68	0.98839	99.89	19.21	0.98896	82.16	15.74	0.98446	89.89
A3	56.19	9.30	0.98852	55.74	9.60	0.98715	63.30	11.46	0.98790	51.45	9.23	0.98263	56.67
A4	39.77	5.56	0.98725	39.38	5.95	0.98570	45.01	7.47	0.98666	36.10	5.86	0.98043	40.07
R1	133.23	25.56	0.98340	132.67	25.51	0.98539	149.08	28.90	0.98270	124.00	23.86	0.98141	134.75
R2	157.89	30.37	0.98237	157.16	30.18	0.98282	176.55	34.09	0.98160	146.83	28.06	0.98261	159.61
R3	167.22	32.03	0.99298	166.42	31.79	0.99292	186.93	35.90	0.99224	155.45	29.50	0.99161	169.01
P1	26.17	2.21	0.97276	25.88	2.67	0.97566	29.87	3.92	0.97280	23.53	2.83	0.97956	26.36
P2	38.07	4.99	0.97719	37.75	5.41	0.97974	43.11	6.88	0.97685	34.69	5.37	0.98336	38.41
P3	61.86	10.31	0.98065	61.48	10.61	0.98290	69.61	12.55	0.98009	57.02	10.17	0.98621	62.49
P4	204.60	40.47	0.98419	203.86	40.08	0.98610	228.56	44.92	0.98347	190.98	37.20	0.98903	207.00

Table A4. The kinetic parameters of the second pyrolysis stage of NOC calculated by CR method at different heating rates.

Model	5 K·min^{-1}			10 K·min^{-1}			15 K·min^{-1}			25 K·min^{-1}			Average
	E_a/kJ·mol^{-1}	ln A/min^{-1}	R^2	E_a/kJ·mol^{-1}	ln A/min^{-1}	R^2	E_a/kJ·mol^{-1}	ln A/min^{-1}	R^2	E_a/kJ·mol^{-1}	ln A/min^{-1}	R^2	E_a/kJ·mol^{-1}
F1	116.72	17.23	0.97878	118.29	17.95	0.99479	119.36	18.30	0.99568	122.92	19.24	0.99989	119.32
F3/2	138.88	21.37	0.95639	141.26	22.18	0.97983	142.57	22.52	0.98114	147.40	23.65	0.99464	142.53
F2	164.17	26.05	0.92872	167.52	26.97	0.95792	169.10	27.32	0.95952	175.42	28.65	0.98058	169.05
F3	222.61	36.77	0.87407	228.25	37.96	0.91068	230.47	38.30	0.91263	240.31	40.13	0.94386	230.41
D1	175.89	26.39	0.99355	176.86	26.88	0.99098	178.38	27.19	0.99065	182.04	28.06	0.97541	178.29
D2	195.13	29.27	0.99393	196.70	29.82	0.99694	198.43	30.14	0.99702	203.02	31.13	0.98767	198.32
D3	219.24	32.21	0.98953	221.64	32.86	0.99881	223.63	33.17	0.99930	229.49	34.34	0.99697	223.50
D4	203.07	29.23	0.99306	204.91	29.82	0.99831	206.73	30.13	0.99853	211.73	31.18	0.99165	206.61
A3/2	73.92	9.71	0.97687	74.90	10.42	0.99439	75.57	10.78	0.99536	77.90	11.58	0.99987	75.57
A2	52.52	5.84	0.97467	53.21	6.54	0.99393	53.67	6.91	0.99499	55.38	7.64	0.99984	53.70
A3	31.12	1.79	0.96907	31.52	2.47	0.99277	31.78	2.85	0.99406	32.87	3.51	0.99976	31.82
A4	20.42	−0.40	0.96112	20.67	0.28	0.99112	20.83	0.66	0.99274	21.62	1.29	0.99962	20.89
R1	82.10	10.66	0.99258	82.50	11.24	0.98938	83.19	11.59	0.98898	84.94	12.28	0.97138	83.18
R2	97.84	12.98	0.99157	98.75	13.61	0.99857	99.61	13.96	0.99889	102.16	14.76	0.99249	99.59
R3	103.78	13.70	0.98857	104.88	14.36	0.99872	105.81	14.71	0.99925	108.67	15.55	0.99650	105.79
P1	11.76	−2.51	0.97700	11.72	−1.87	0.96276	11.79	−1.49	0.96108	12.12	−0.93	0.90878	11.85
P2	19.58	−0.75	0.98532	19.59	−0.12	0.97711	19.72	0.26	0.97613	20.21	0.83	0.94166	19.78
P3	35.21	2.33	0.98986	35.31	2.95	0.98482	35.59	3.32	0.98421	36.40	3.92	0.96013	35.63
P4	129.00	18.59	0.99325	129.68	19.13	0.99049	130.78	19.46	0.99013	133.49	20.24	0.97416	130.74

Table A5. The kinetic parameters of the first pyrolysis stage of NOC calculated by KC method at different heating rates.

Model	5 K·min^{-1}			10 K·min^{-1}			15 K·min^{-1}			25 K·min^{-1}			Average
	E_a/kJ·mol^{-1}	ln A/min^{-1}	R^2	E_a/kJ·mol^{-1}	ln A/min^{-1}	R^2	E_a/kJ·mol^{-1}	ln A/min^{-1}	R^2	E_a/kJ·mol^{-1}	ln A/min^{-1}	R^2	E_a/kJ·mol^{-1}
F1	186.81	34.57	0.99033	186.08	34.26	0.98925	209.25	38.73	0.98976	173.99	31.71	0.98577	189.03
F3/2	221.80	42.11	0.97823	220.79	41.59	0.97576	248.24	46.81	0.97797	206.28	38.36	0.96937	224.28
F2	261.84	50.72	0.95925	260.50	49.96	0.95563	292.86	56.05	0.95933	243.19	45.96	0.94681	264.60
F3	354.50	70.63	0.91623	352.38	69.31	0.91101	396.13	77.41	0.91679	328.57	63.52	0.89889	357.90
D1	275.17	51.79	0.98454	274.48	51.11	0.98644	307.63	57.32	0.98384	257.66	47.13	0.98933	278.74
D2	305.25	57.61	0.99053	304.35	56.75	0.99154	341.13	63.60	0.98977	285.53	52.21	0.99257	309.07
D3	343.15	64.29	0.99329	341.97	63.21	0.99323	383.34	70.86	0.99258	320.56	57.95	0.99201	347.26
D4	317.72	58.80	0.99214	316.74	57.87	0.99278	355.02	64.98	0.99139	297.06	53.09	0.99302	321.64
A3/2	121.10	21.00	0.98976	120.63	21.03	0.98862	136.08	24.15	0.98924	112.57	19.63	0.98990	122.60
A2	88.25	14.22	0.98915	87.90	14.41	0.98795	99.49	16.85	0.98868	81.86	13.60	0.98395	89.38
A3	55.39	7.43	0.98776	55.17	7.80	0.98640	62.91	9.56	0.98741	51.15	7.56	0.98175	56.16
A4	38.97	4.04	0.98608	38.81	4.49	0.98455	44.61	5.91	0.98593	35.80	4.54	0.97908	39.55
R1	132.43	22.83	0.98334	132.10	22.83	0.98539	148.68	26.15	0.98273	123.70	21.31	0.98844	134.23
R2	157.09	27.47	0.98228	156.59	27.33	0.98275	176.15	31.17	0.98156	146.53	25.34	0.98251	159.09
R3	166.42	29.08	0.99286	165.85	28.89	0.99280	186.54	32.92	0.99216	155.15	26.72	0.99147	168.49
P1	25.37	1.11	0.97204	25.31	1.63	0.97542	29.47	2.77	0.97282	23.23	1.94	0.97969	25.845
P2	37.27	3.52	0.97683	37.18	3.99	0.97964	42.72	5.36	0.97690	34.39	4.09	0.98347	37.89
P3	61.06	8.35	0.98049	60.91	8.70	0.98287	69.21	10.56	0.98013	56.72	8.40	0.98629	61.98
P4	203.80	37.31	0.98416	203.29	36.97	0.98610	228.16	41.73	0.98348	190.68	34.22	0.98905	206.48

Table A6. The kinetic parameters of the second pyrolysis stage of NOC calculated by KC method at different heating rates.

Model	5 K·min^{-1}			10 K·min^{-1}			15 K·min^{-1}			25 K·min^{-1}			Average
	E_a/kJ·mol^{-1}	ln A/min^{-1}	R^2	E_a/kJ·mol^{-1}	ln A/min^{-1}	R^2	E_a/kJ·mol^{-1}	ln A/min^{-1}	R^2	E_a/kJ·mol^{-1}	ln A/min^{-1}	R^2	E_a/kJ·mol^{-1}
F1	117.99	15.03	0.97873	119.71	15.76	0.99468	120.88	16.12	0.99558	124.56	17.05	0.99990	120.79
F3/2	140.15	19.00	0.95655	142.68	19.82	0.97984	144.10	20.17	0.98117	149.04	21.28	0.99458	143.99
F2	165.44	23.51	0.92913	168.94	24.44	0.95815	170.63	24.79	0.95979	177.06	26.10	0.98065	170.52
F3	223.88	33.92	0.87480	229.67	35.12	0.91125	232.00	35.46	0.91326	241.96	37.27	0.94425	231.88
D1	177.16	23.78	0.99365	178.28	24.29	0.99130	179.91	24.61	0.99099	183.68	25.48	0.97614	179.76
D2	196.40	26.56	0.99392	198.12	27.13	0.99706	199.96	27.45	0.99715	204.66	28.44	0.98807	199.79
D3	220.51	29.38	0.98948	223.06	30.04	0.99880	225.16	30.36	0.99929	231.13	31.53	0.99710	224.97
D4	204.34	26.48	0.99303	206.33	27.08	0.99836	208.25	27.40	0.99860	213.37	28.45	0.99194	208.07
A3/2	75.19	7.97	0.97683	76.32	8.69	0.99422	77.10	9.06	0.99521	79.54	9.85	0.99989	77.04
A2	53.79	4.44	0.97465	54.63	5.15	0.99369	55.20	5.53	0.99478	57.03	6.25	0.99988	55.16
A3	32.39	0.91	0.96927	32.94	1.61	0.99239	33.31	2.00	0.99372	34.51	2.64	0.99985	33.29
A4	21.69	−0.85	0.96193	22.09	−0.16	0.99061	22.36	0.23	0.99228	23.26	0.84	0.99981	22.35
R1	83.38	8.81	0.99283	83.92	9.41	0.99014	84.71	9.77	0.98979	86.58	10.46	0.97313	84.65
R2	99.12	10.96	0.99149	100.17	11.61	0.99863	101.14	11.97	0.99897	103.80	12.76	0.99303	101.06
R3	105.05	11.61	0.98846	106.30	12.29	0.99868	107.34	12.65	0.99923	110.31	13.48	0.99679	107.25
P1	13.03	−2.41	0.98175	13.14	−1.75	0.97440	13.32	−1.35	0.97365	13.76	−0.80	0.93443	13.31
P2	20.85	−1.16	0.98728	21.01	−0.51	0.98225	21.25	−0.12	0.98168	21.85	0.45	0.95328	21.24
P3	36.48	1.33	0.99064	36.73	1.97	0.98703	37.12	2.35	0.98658	38.04	2.95	0.96518	37.09
P4	130.27	16.30	0.99339	131.10	16.85	0.99094	132.31	17.19	0.99061	135.13	17.97	0.97520	132.20

References

1. He, Z.G.; Li, Q.; Fang, J. The Solutions and Recommendations for Logistics Problems in the Collection of Medical Waste in China. *Procedia Environ. Sci.* **2016**, *31*, 447–456. [CrossRef]
2. Wilson, A.J.; Nayak, S. Disinfection, sterilization and disposables. *Anaesth. Intensive Care* **2016**, *17*, 475–479. [CrossRef]
3. Deng, N.; Zhang, Y.F.; Wang, Y. Thermogravimetric analysis and kinetic study on pyrolysis of representative medical waste composition. *Waste Manag.* **2007**, *28*, 1572–1580. [CrossRef] [PubMed]
4. Sharuddin, S.D.A.; Abnisa, F.; Daud, W.M.A.W.; Aroud, M.K. A review on pyrolysis of plastic wastes. *J. Environ. Manag.* **2016**, *115*, 308–326. [CrossRef]
5. Bridgwater, A.V. Review of fast pyrolysis of biomass and product upgrading. *Biomass Bioenergy* **2012**, *38*, 68–94. [CrossRef]
6. Abnisa, F.; Daud, W.M.A.W. A review on co-pyrolysis of biomass: An optional technique to obtain a high-grade pyrolysis oil. *Energy Convers. Manag.* **2014**, *87*, 71–85. [CrossRef]
7. Wang, Z.; Xie, T.; Ning, X.Y.; Liu, Y.C.; Wang, J. Thermal degradation kinetics study of polyvinyl chloride (PVC) sheath for new and aged cables. *Waste Manag.* **2019**, *99*, 146–153. [CrossRef]
8. Aboulkas, A.; El harfi, K.; El Bouadili, A. Thermal degradation behaviors of polyethylene and polypropylene. Part I: Pyrolysis kinetics and mechanisms. *Energy Convers. Manag.* **2010**, *51*, 1363–1369. [CrossRef]
9. Xu, F.F.; Wang, B.; Yang, D.; Hao, J.H.; Qiao, Y.Y.; Tian, Y.Y. Thermal degradation of typical plastics under high heating rate conditions by TG-FTIR: Pyrolysis behaviors and kinetic analysis. *Energy Convers. Manag.* **2018**, *171*, 1106–1115. [CrossRef]
10. Han, B.; Wu, Y.L.; Feng, W.; Chen, Z.; Yang, M.D. Kinetic Study of PVC Pyrolysis in Air by Thermogravimetric Analysis Using the Friedman Method. *Adv. Mater. Res.* **2012**, *427*, 64–69. [CrossRef]
11. Nisar, J.; Khan, M.A.; Ali, G.; Iqbal, M.; Shah, A.; Shah, M.R.; Sherazi, S.T.H. Pyrolysis of polypropylene over zeolite mordenite ammonium: Kinetics and products distribution. *J. Polym. Eng.* **2019**, *39*, 785–793. [CrossRef]
12. Tewarson, A.; Macaione, D.P. Polymer and composites-An examination of ire spread and generation of heat and fire products. *J. Fire Sci.* **1993**, *11*, 421–441. [CrossRef]
13. Ushkov, V.A.; Abramov, V.V.; Grigor'eva, L.S.; Kir'yanova, L.V. Thermal stability and fire hazard of epoxy polymer pastes. *Stroit. Mater.* **2011**, *12*, 68–71.
14. Hassel, R.L.; Baker, K.F. Evaluation of potential polymer safety hazards by thermal analysis. *Soc. Plast. Eng. Tech. Pap.* **1978**, *24*, 384–386.
15. Huang, Y.J.; Tu, C.H.; Chao, H.R.; Chen, H.T. Pyrolysis and Oxidation Kinetics of Medical Wastes. *Environ. Technol.* **2006**, *27*, 153–158. [CrossRef] [PubMed]
16. Yan, J.H.; Zhu, H.M.; Jiang, X.G.; Chi, Y.; Cen, K.F. Analysis of volatile species kinetics during typical medical waste materials pyrolysis using a distributed activation energy model. *J. Hazard. Mater.* **2009**, *162*, 646–651. [CrossRef] [PubMed]
17. Deng, N.; Wang, W.W.; Cui, W.Q.; Zhang, Y.F.; Ma, H.T. Thermogravimetric characteristics and different kinetic models for medical waste composition containing polyvinyl chloride-transfusion tube. *J. Cent. South Univ.* **2014**, *21*, 1034–1043. [CrossRef]
18. Qin, L.B.; Han, J.; Zhao, B.; Chen, W.S.; Xing, F.T. The kinetics of typical medical waste pyrolysis based on gaseous evolution behaviour in a micro-fluidised bed reactor. *Waste Manag. Res.* **2018**, *36*, 1073–1082. [CrossRef]
19. Jiang, L.; Zhang, D.; Li, M.; He, J.J.; Gao, Z.H.; Zhou, Y.; Sun, J.H. Pyrolytic behavior of waste extruded polystyrene and rigid polyurethane by multi kinetics methods and Py-GC/MS. *Fuel* **2018**, *222*, 11–20. [CrossRef]
20. Jiang, L.; Xiao, H.H.; He, J.J.; Sun, Q.; Gong, L.; Sun, J.H. Application of genetic algorithm to pyrolysis of typical polymers. *Fuel. Process. Technol.* **2015**, *138*, 48–55. [CrossRef]
21. Akerblom, I.E.; Ojwang, D.O.; Grins, J.; Svensson, G. A thermogravimetric study of thermal dehydration of copper hexacyanoferrate by means of model-free kinetic analysis. *J. Therm. Anal. Calorim.* **2017**, *129*, 721–731. [CrossRef]
22. Grigiante, M.; Brighenti, M.; Antolini, D. Analysis of the impact of TG data sets on activation energy (E_a). *J. Therm. Anal. Calorim.* **2017**, *129*, 553–565. [CrossRef]
23. Ankita, S.; Namrata, C.; Neeraj, M. Calorimetric studies of crystallization for multi-component glasses of Se–Te–Sn–Ag (STSA) system using model-free and model-fitting non-isothermal methods. *J. Therm. Anal. Calorim.* **2017**, *128*, 907–914.
24. Janković, B.; Mentus, S. Model-fitting and model-free analysis of thermal decomposition of palladium acetylacetonate [Pd(acac) 2]. *J. Therm. Anal. Calorim.* **2008**, *94*, 395–403. [CrossRef]
25. Flynn, J.H.; Wall, L.A. A quick, direct method for the determination of activation energy from thermogravimetric data. *Polym. Lett.* **1966**, *4*, 323–328. [CrossRef]
26. Ozawa, T. A new method of analyzing thermogravimetric data. *Bull. Chem. Soc. Jpn.* **1965**, *38*, 1881–1886. [CrossRef]
27. He, K. Reaction kinetics in differential thermal analysis. *Anal. Chem.* **1957**, *29*, 1702–1706.
28. Akahira, T.; Sunose, T. Method of determining activation deterioration constant of electrical insulating materials. *Res. Rep. Chiba Inst. Technol.* **1971**, *16*, 22–31.
29. Friedman, H.L. Kinetics of thermal degradation of char-forming plastics from thermogravimetry. Application to a phenolic plastic. *J. Polym. Sci. Part C* **1964**, *6*, 183–195. [CrossRef]
30. Coats, A.W.; Redfern, J.P. Kinetic parameters from thermogravimetric data. *Nature* **1964**, *201*, 68–69. [CrossRef]

31. Kennedy, J.A.; Clark, S.M. A New Method for the Analysis of Non-Isothermal DSC and Diffraction Data. *Thermochim. Acta* **1997**, *307*, 27–35. [CrossRef]
32. Doyle, C.D. Estimating isothermal life from thermogravimetric data. *J. Appl. Polym. Sci.* **1962**, *6*, 639–642. [CrossRef]
33. Soganciogl u, M.; Yel, E.; Ahmetli, G. Behaviour of waste polypropylene pyrolysis char-based epoxy composite materials. *Environ. Sci. Pollut. Res.* **2019**, *27*, 3871–3884. [CrossRef] [PubMed]
34. Zhou, R.; Huang, B.; Ding, Y.; Li, W.; Mu, J. Thermal Decomposition Mechanism and Kinetics Study of Plastic Waste Chlorinated Polyvinyl Chloride. *Polymers* **2019**, *11*, 2080. [CrossRef] [PubMed]
35. Al-Salem, S.M.; Antelava, A.; Constantinou, A.; Manos, G.; Dutta, A. A review on thermal and catalytic pyrolysis of plastic solid waste (PSW). *J. Environ. Manag.* **2017**, *197*, 177–198. [CrossRef]
36. Kunwar, B.; Cheng, H.N.; Chandrashekaran, S.R.; Sharma, B.K. Plastics to fuel: A review. *Renew. Sustain. Energy Rev.* **2016**, *54*, 421–428. [CrossRef]
37. Yang, K.K.; Wang, X.L.; Wang, Y.Z.; Wu, B.; Jin, Y.D.; Yang, B. Kinetics of thermal degradation and thermal oxidative degradation of poly(p-dioxanone). *Eur. Polym. J.* **2003**, *39*, 1567–1574. [CrossRef]
38. Lesnikovich, A.; Levchik, S. A method of finding invariant values of kinetic parameters. *J. Therm. Anal. Calorim.* **1983**, *27*, 89–93. [CrossRef]
39. Vyazovkin, S. A unified approach to kinetic processing of nonisothermal data. *Int. J. Chem. Kinet.* **1996**, *28*, 95–101. [CrossRef]
40. Koga, N.; Tanaka, H. Accommodation of the actual solid-state process in the kinetic model function. Part 2. Applicability of the empirical kinetic model function to diffusion-controlled reactions. *Thermochim. Acta* **1996**, *282*, 69–80. [CrossRef]
41. Cao, H.Q.; Lin, J.; Duan, Q.L.; Zhang, D.; Chen, H.D.; Sun, J.H. An experimental and theoretical study of optimized selection and model reconstruction for ammonium nitrate pyrolysis. *J. Hazard. Mater.* **2019**, *364*, 539–547. [CrossRef] [PubMed]